39th ERF, September 2–5, 2014, Southampton, UK

019

AN EXPERIMENTAL SET UP FOR THE STUDY OF HELICOPTER AND BUILDING AERODYNAMIC INTERACTION

G. Gibertini*, C. Clavel, D. Grassi, C. Parolini, D. Zagaglia and A. Zanotti

Politecnico di Milano – Dipartimento di Scienze e Tecnologie Aerospaziali
Via La Masa 34, 20156 Milano – Italy
e–mail: *giuseppe.gibertini@polimi.it

Keywords: Rotorcraft, Aerodynamics, Vortex Interaction, Particle Image Velocimetry (PIV), Ground Obstacles.

Abstract

In the present study, a new experimental setup for the investigation of the aerodynamic interaction between a helicopter and ground obstacles is presented and assessed. The motorised helicopter model, which includes the fuselage, can be positioned in different positions relative to a model building in order to replicate different configurations. Moreover the current setup can also be used in a wind tunnel in order to replicate interference effects in windy conditions. The use of a helicopter model with a six-component balance and a building model with several pressure taps allows a database to be compiled for the loads on the helicopter and obstacle. A physical interpretation of the flow phenomena can be obtained through analysis of the obstacle pressure measurements and particle image velocimetry surveys of relevant configurations.

Nomenclature

A	rotor area
c	blade section model chord
CFD	Computational Fluid Dynamics
C_p	pressure coefficient
C_t	thrust coefficient, $\equiv \frac{T}{\rho V_{TIP}^2 A}$
C_q	torque coefficient, $\equiv \frac{Q}{\rho V_{TIP}^2 AR}$
DLR	German Aerospace Center
FAA	Federal Aviation Administration
FM	Figure of Merit $\equiv \frac{C_t^{3/2}}{C_q\sqrt{2}}$
IGE	In Ground Effect
IHST	International Helicopter Safety Team
JHSAT	Joint Helicopter Safety Analysis Team
M	Mach number
MT	Momentum Theory
OGE	Out of Ground Effect
P_∞	far-field Pressure
PIV	Particle Image Velocimetry
R	rotor radius
RPM	revolutions per minute
Re_{TIP}	Reynolds number at the blade tip, $\equiv \frac{V_{\mathrm{TIP}}c}{\nu}$
$\|U\|$	velocity magnitude
V_{TIP}	tip blade speed, $\equiv \Omega R$
V_{IND}	Rotor induced velocity
X	longitudinal coordinate
Y	span-wise coordinate
Z	vertical coordinate

1 INTRODUCTION

The helicopter is a very versatile flying machine that is often required to operate close to vertical obstacles such as buildings, ships and mountain walls. The danger intrinsic to these flight conditions is evident in the accident database [1] collected by the Joint Helicopter Safety Analysis Team (JHSAT) for the International Helicopter Safety Team (IHST). This study highlighted the fact that most helicopter accidents (61.4%) occur during take-off and landing – i.e. generally in the presence of ground obstacles. These situations can be further complicated under windy conditions, particularly when the helicopter flies inside the turbulent and extremely unsteady wake generated by an obstacle [2].

Therefore, the aerodynamic interaction between a helicopter and obstacles is a quite important research subject, and several numerical and experimental studies have been published in the scientific literature. The most commonly investigated situation in the recent literature has been the helicopter in proximity to ship decks.

For instance, Crozon et al. [3] analysed different numerical approaches for the simulation of rotors flow field in a ship air wake, while Alpman et al. [4] were able to fully couple Computational Fluid Dynamics (CFD) simulations with flight dynamics for the study of similar configurations.

Lee and Zan [6, 7] and Zan [8] performed experiments to measure the loads acting on a helicopter in the wake of a scaled frigate for different configurations: isolated rotor, isolated fuselage, and rotor with fuselage. Timm [5] was the first to observe the flow recirculation induced by the interaction between the rotor and obstacle through flow visualizations. Recently, the use of particle image velocimetry (PIV) has enabled the quantitative analysis of this interacting flow field; for example Nacakli and Landman [9] examined the interaction between a helicopter and the air wake of a frigate. Rajagopalan et al. [10] and Quinliven and Long [11] compared numerical and experimental results for the topology of the interacting flow field using scaled models of helicopter and buildings. In contrast, Polsky and Wilkinson [12] compared the results of a numerical study with those of an experiment on a full-scale helicopter in the proximity of a hangar.

Despite the relative abundance of numerical and experimental works, a systematic study of the aerodynamic phenomena involved which considers a wide set of cases is lacking. Moreover, most of these investigations have focused on the effect on the helicopter performance and handling qualities, and *de facto* have neglected the corresponding load effects on the obstacle.

This paper aims at presenting a new experimental setup useful for these kind of investigations and its potentialities. To do so, after a thorough description of the hardware and instrumentation adopted, the results of a preliminary series of tests reproducing hovering flight

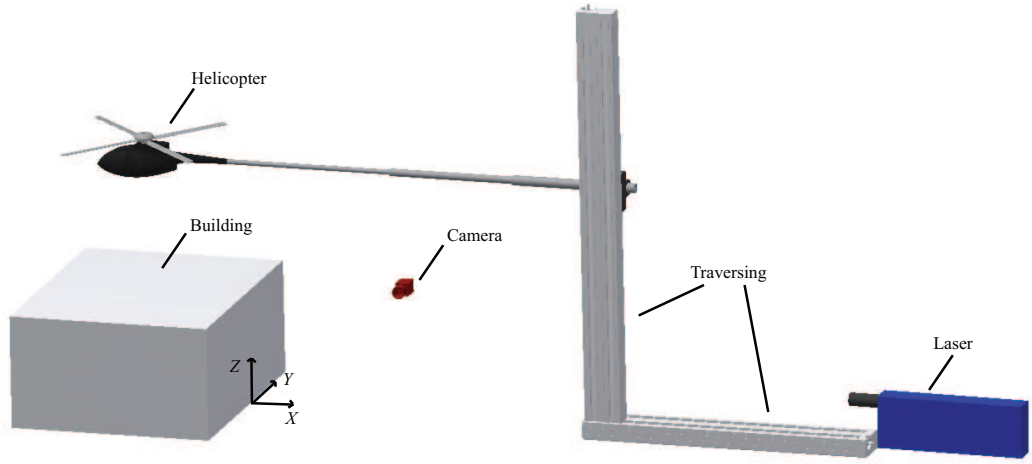

Figure 1: Layout of helicopter–building interaction experiment and reference system (including PIV set up).

conditions at different positions with respect to a simplified volume with a parallelepiped shape are presented. This parallelpiped model was courteously made available by DLR in the frame of a collaboration that should continue in the future under the auspices of the GARTEUR organisation [13]. Scale effects were unavoidably present in the experiment compared to similar full-scale conditions; however the scaled-down tests were essential for producing an accurate and repeatable database, because laboratory conditions are much more stable and controllable. Measurement of both the loads acting on the rotor and the pressure distributions over the external surfaces of the obstacle revealed information on the mutual effects of the aerodynamic interaction. PIV was used to investigate the details of the interacting flow field under several conditions of interest.

2 EXPERIMENTAL SET UP

The test rig essentially consists of a helicopter model, inspired by the MD-500, and a geometric obstacle which represents an ideal building. The helicopter model is held by a horizontal

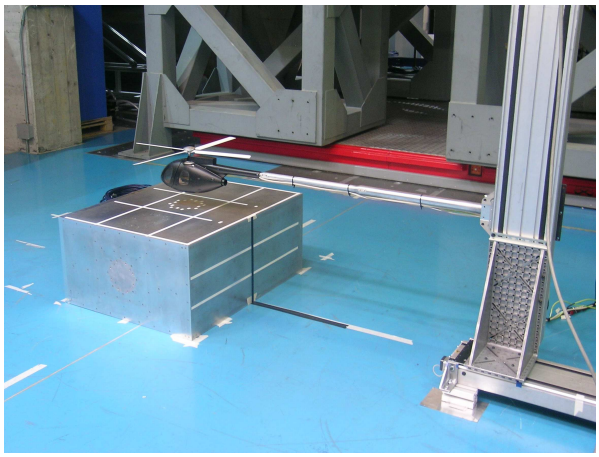

Figure 2: Photo of the experimental rig.

strut fixed to a system of two motorised orthogonal sliding guides to allow the relative position to be changed with respect to the obstacle along the vertical and longitudinal directions of the fuselage. Figures 1 and 2 show the set up of the helicopter–building interaction experiment as well as the reference system used in the present study. For the coordinate reference system, the X-Z plane is aligned with the mid-span plane of the building model and the X-Y plane is aligned with the floor. The origin of the

reference system is located on the floor, at the mid-span of the front face. As shown in Figure 5, for the considered low-rise configuration of the building, the Y axis lies on the longer side of the building base.

2.1 Helicopter model

Figure 3 shows the helicopter model (rotor and fuselage). The rotor has four untwisted and untapered rectangular blades with a chord of $c = 0.032$ m and radius of $R = 0.375$ m, at a $1 : 10.7$ scale ratio. The NACA 0012 airfoil is used. No swash plate is present, so the blade pitch angle is fixed to 10°. The rotational speed of the rotor can be controlled as needs dictate by means of a brush-less low-voltage electrical motor with an electronic controller. A nominal rotational speed of 2480 rpm was maintained during all the tests for the results that will presented afterwards. The resulting Mach number and Reynolds number at the blade tip were $M_{\mathrm{TIP}} = 0.286$ and $Re_{\mathrm{TIP}} = 214,000$, respectively.

The forces and moments acting on the rotor are measured with a six-component balance nested inside the fuselage. A Hall effect sensor produces one signal per revolution to act as the feedback signal for RPM control. Figure 4 shows a schematic of the helicopter model layout.

The fixed rotor described above does not represent all of the details of the complex phenomena which occur in an articulated rotor, e.g. the flapping motion. However, in the present experiment the model was kept in a fixed position (hovering flight); therefore, the forward flight effects that strongly affect blade flapping were not present. Hence, the behaviour of the interaction between the helicopter model and the obstacle can be considered adequately representative of a general case. The choice of a fixed rotor was also motivated by the intention of obtaining well-defined reference data for comparison with numerical simulations.

With regard to the inexact matching of M_{TIP}, the aim of the present study was to analyse the interaction between the rotor wake and obstacle; therefore, matching Mach number at tip was not essential, because the topology of the wake is not greatly influenced by such a parameter ([14],[15]). A larger effect of the small-scale can be expected because of the low Re_{TIP}. At low Reynolds numbers, the blade profile drag coefficient increases; this produces an higher resistant torque, which results in a swirl stronger than in full-scale condition. Nevertheless note that the employed model was able to reach a Reynolds number higher than the one achieved in similar investigations by [10] and [11], and practically equal to that obtained by [6]. The model dimensions were limited by the need to avoid interference by the surrounding test environment.

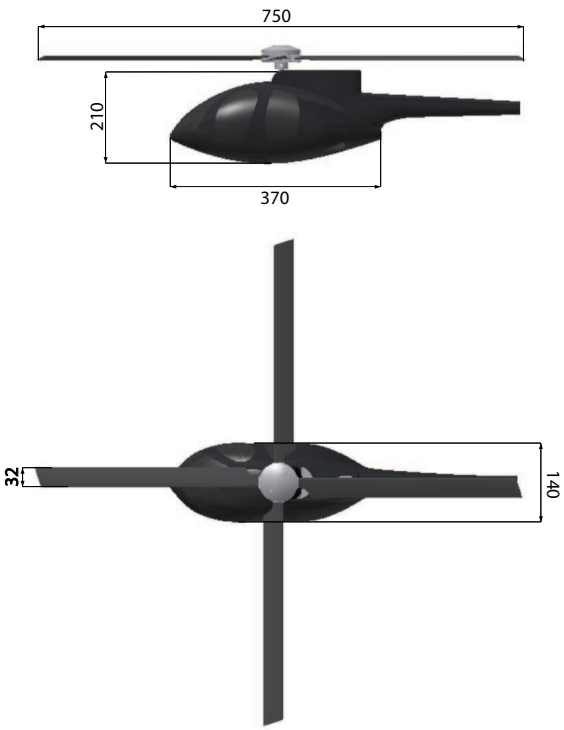

Figure 3: Sketch of helicopter model (dimensions in mm).

2.2 Building model

The building model is a parallelepiped with sharp edges courteously made available by DLR. It comprises an internal structure of aluminium alloy square tubes holding external aluminium alloy plates and it is equipped with 150 pressure taps (see Fig. 5), not equally distributed on the different faces. The dimensions of the parallelepiped are 0.45 m × 0.8 m × 1.0 m. The building can be leaned over dif-

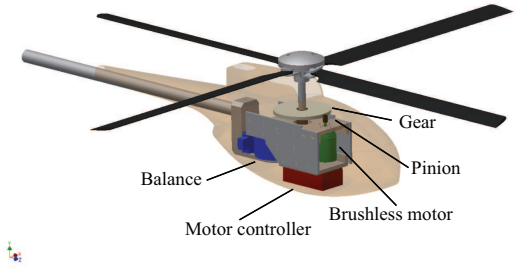

Figure 4: Sketch of helicopter model and nested instrumentation.

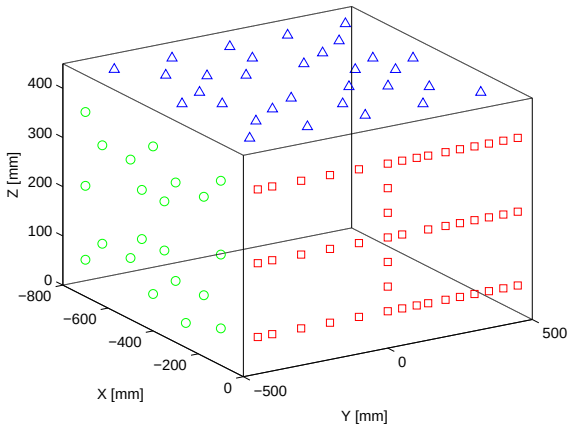

Figure 5: Pressure tap locations on model building. The top, side and front plates are characterised by triangle, circle and square markers respectively.

ferent faces, allowing to consider several building configurations (e.g. low-rise and high-rise). The experimental results that are presented in the present paper were obtained considering a low-rise configuration (i.e. with the 0.8 m $\times$ 1.0 m face lying on the ground). For such configuration 31 pressure taps were considered on the top plate , 21 on the side plate and 48 on the front plate. The remaining taps were located on the other three faces, which are not considered in the present study.

The pressures are acquired by means of five 32-port scanners by Pressure System Inc. embedded inside the building model. The declared accuracy of these pressure transducers led to an uncertainty in pressure coefficients of $\pm$ 0.15, but previous experience and some tests carried out before the experiment led to a C_p uncertainty of less than 0.1.

2.3 PIV set up

The PIV system comprised a Litron NANO-L-200-15 Nd:Yag double-pulse laser with an output energy of 200 mJ and wavelength of 532 nm, and an Imperx ICL-B1921M CCD camera with a 12-bit, 1952 $\times$ 1112 pixel array. For the present application, the laser was positioned on the floor so that the laser sheet was aligned with the X-Z plane (see the layout in Fig. 1). The camera line of sight was positioned perpendicular to the laser sheet. As shown in Figure 6, the PIV measurement window was 300 mm $\times$ 400 mm. In order to achieve better resolution of the image pairs, the measurement area comprised two adjacent windows, one on top of the other, with a small overlapping band between them. The synchronisation of the two laser pulses with the image pair exposure was controlled by a six-channel Quantum Composer QC9618 pulse generator. A PIVpart30 particle generator by PIVTEC with Laskin atomizer nozzles was used for the seeding, which consisted of small oil droplets with diameters of 1-2 μm. The image pair analysis was carried out using PIVviev 2C software [16], which was developed by PIVTEC in close cooperation with the PIV-Group of DLR.

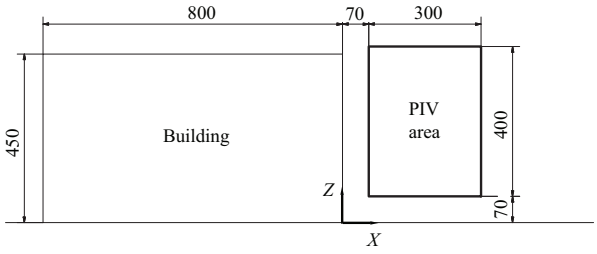

Figure 6: Schematic of PIV measurement area (dimensions in mm).

2.4 The wind tunnel

The preliminary results presented in this paper were obtained without considering external wind, as an assessment of the experimental setup. However its potentialities can be enhanced through wind tunnel surveys in order to study the helicopter-obstacle interaction

in windy conditions, taking advantage of The large wind tunnel of Politecnico di Milano.

This facility has two different test chambers: a 4m x 3.84m aeronautical test section (downstream a settling chamber and a contraction) characterized by a very good flow quality, and a 13.84m x 3.84m wind engineering test chamber (located in the return duct) with a less regular flow. For the investigation of the interference between the helicopter and the building model, the latter test chamber could be used, in order to reduce to the minimum the blockage and the interference with the surroundings. The flow inside the wind engineering test chamber is characterized by a stable floor boundary layer thickness in the order of 0.4m and a mean turbulence level in the order of 2%. For further details, please see [17]

3 TEST MATRIX AND EXPERIMENTAL PROCEDURE

As mentioned in Section 1, each test comprised a measurement where the model was kept in a defined position with respect to the building model. Thus, the tests essentially reproduced hovering flight conditions (although not exactly trimmed).

The Tests presented in this paper were carried out with the parallelepiped leaned on the 0.8 m $\times$ 1 m face to represent a low-rise building. With respect to the reference systems shown in Fig. 1, a vertical sweep, where X and Y were constant and a horizontal sweep, where Z and Y were constant, were carried out. Table 1 lists the parameters used for the different test conditions. The coordinates which identify the helicopter model position refer to the intersection point between the rotor shaft axis and rotor disk.

3.1 Load and pressure measurements

In order to reduce the balance thermal drifts, each test point corresponded to a single run where the motor was started from rest and then stopped again at the end of the acquisition. The acquisition took place over 5 s long and was preceded by 10 s of flow stabilisation. The balance zeroes were acquired immediately before and after each run and the mean of these two readings was used to account for the balance thermal drift. However, because of the short run time, this zero drift was quite small. The rotational speed was set equal to 2480 rpm (corresponding to $M_{\mathrm{TIP}} = 0.286$), although drifts of up to 30 rpm occurred during the tests. Thus, the actual RPM value was continuously acquired so that the thrust and torque coefficients would be correctly computed. Four runs were carried out for each measurement point, and the obtained results were averaged.

A similar procedure was adopted for pressure measurements; however the acquisition time was set to 10 s in order to filter out, by averaging over a longer time, the pressure fluctuations due to the unsteadiness. The pressure results were represented by the pressure coefficient C_p:

$$C_p = \frac{P - P_\infty}{\frac{1}{2}\rho V_{\mathrm{IND}}^2}, \tag{1}$$

where P_∞ is the far-field pressure and V_{IND} is the estimated rotor-induced velocity according to the Momentum Theory (MT) [18] and is defined as $V_{\mathrm{IND}} = V_{\mathrm{TIP}}\sqrt{\frac{C_{t,OGE}}{2}}$.

4 TEST RESULTS AND DISCUSSION

Test 0 was intended to be a repeatability test; it consisted of several repetitions of the load measurements with the helicopter model in a fixed position in order to check the precision of the measurement chain. This test was carried out without the building model at a height of $Z/R = 5$, i.e. out of ground effect (OGE) condition. After 30 runs, the average thrust coefficient was $C_{t_{OGE}} = 0.00705$, and the torque coefficient was $C_{q_{OGE}} = 0.000750$. The standard deviation was 0.3% for both the thrust and torque coefficients; thus, the measurement showed a high level of repeatability.

The first sweep in the Z (vertical) direction (test 1 of Table 1) was carried out without obstacles to produce a reference condition for comparison with the obstacle effects. Figure

N	Building Configuration		Sweep Axis			First Point			Last Point		
	No Build.	Build.	X	Y	Z	X/R	Y/R	Z/R	X/R	Y/R	Z/R
0	×					$\cdot/\cdot$	$\cdot/\cdot$	5	$\cdot/\cdot$	$\cdot/\cdot$	5
1	×				×	$\cdot/\cdot$	$\cdot/\cdot$	1	$\cdot/\cdot$	$\cdot/\cdot$	5
2		×	×			-1	0	2	1	0	2

Table 1: Test matrix

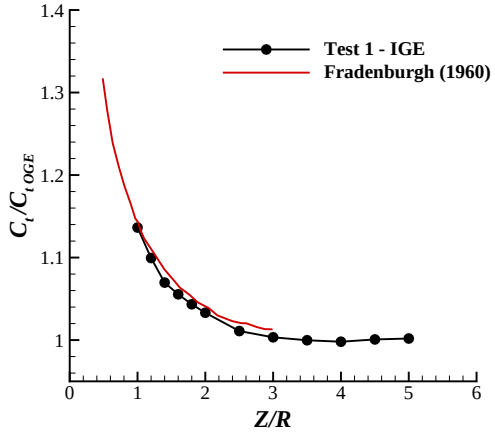

(a) Thrust coefficient

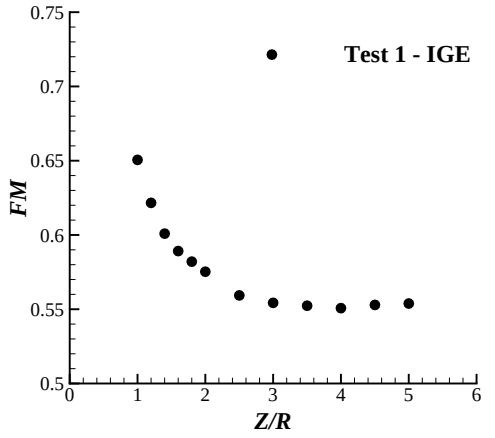

(b) Figure of merit

Figure 7: Ground effect test without building model. Results were for different heights from the ground and compared with data from literature

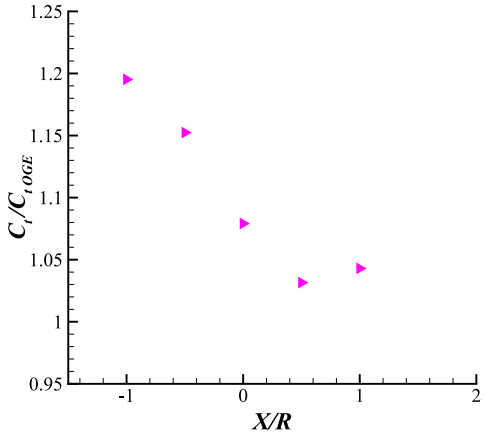

(a) Thrust coefficient

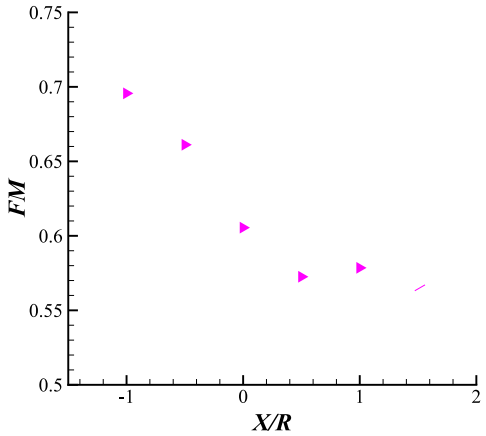

(b) Figure of merit

Figure 8: Results of C_t and FM for test 2 (horizontal sweep at $Y/R = 0$, $Z/R = 2$).

7(a) plots the results of this reference test in terms of $C_t/C_{t_{OGE}}$ and compares them with those obtained by Fradenburgh [19]. Fradenburgh conducted ground effect tests using a two-bladed rotor, with a diameter of $D = 2ft \simeq 0.6m$ and chord of $c = 2in \simeq 5cm$ operating at V_{TIP} of approximately $600ft/s$, $RPM \simeq 5800$. Despite the difference in geometric and operating conditions, the present results showed good agreement and thus validated the experimental setup. Figure 7(b) presents the results in terms of figure of merit (FM). Under the OGE condition, $FM = 0.564$. This is not far from the typical FM for helicopters and is within the expected order of magnitude for a model of this scale without a blade sweep.

Test 2 comprised the building model and it considered a set of points on a horizontal line on the symmetry plane at $Z/R = 2$. These points can represent a slow horizontal approach. Figure 8 shows the results for X/R varying from -1 to 1. The first considered position was $X/R = -1$; the entire rotor disk was over the obstacle, although not exactly centred with respect to the building roof (the centre of the roof was at $X/R = -1.07$). For this configuration, $C_t/C_{t_{OGE}} = 1.195$, according to the results of test 1 considering the distance between the helicopter and the upper surface of the building. Away from the building centre, $C_t/C_{t_{OGE}}$ decreased according to the minor percentage of the rotor projection lying on top of the building. $C_t/C_{t_{OGE}}$ was 1.03 for the outer position, just as it was in test 1 at the same height. Figure 9 presents the pressure results. The pressure distribution with the model positioned at $X/R = -1$ highlights a high-pressure region corresponding to the impingement area of the rotor wake. When the rotor centre lay exactly on the building edge ($X/R = 0$), the pressure distributions on the different faces of the building indicated the presence of a complex flow structure that was markedly asymmetrical. The diagonal pattern on the front face was probably related to the helicoidal structure of the rotor wake. Although the adopted measurement system did not allow a thorough evaluation of the pressure fluctuations, the single samples acquired on this face presented a higher variability than in all of the other cases. For $X/R = 1$ the helicopter effect was only apparent on the front face, since an overpressure is evident where the wake, deflected by the ground, impinged.

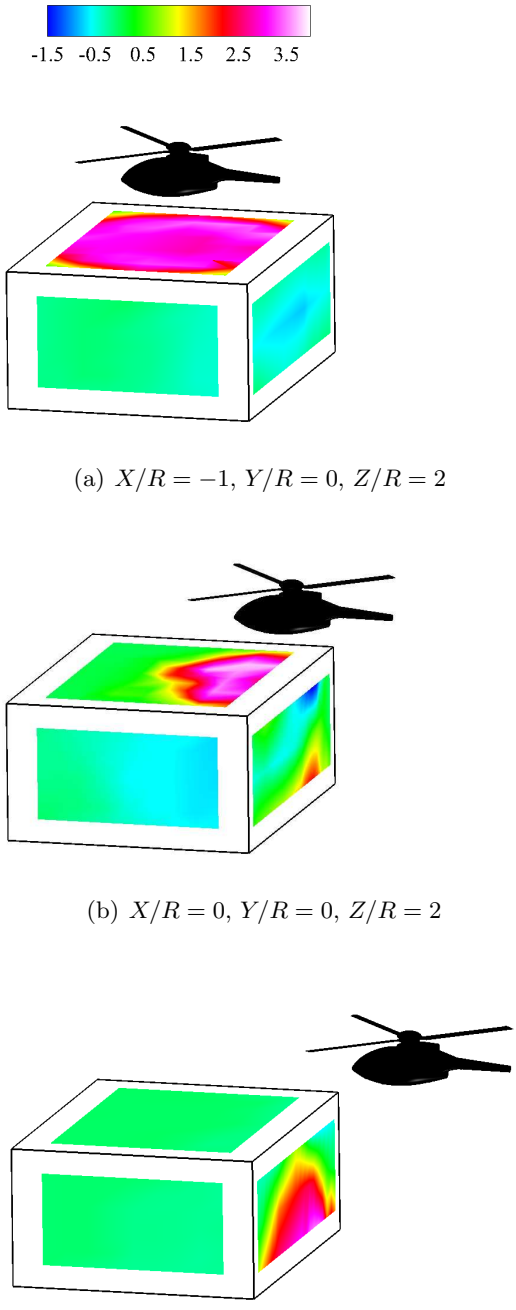

(a) $X/R = -1$, $Y/R = 0$, $Z/R = 2$

(b) $X/R = 0$, $Y/R = 0$, $Z/R = 2$

(c) $X/R = 1$, $Y/R = 0$, $Z/R = 2$

Figure 9: Pressure distribution over building model under test 2 conditions: C_p contours.

4.1 PIV measurements

PIV was used to observe the interacting flow field on the building symmetry plane ahead of the building front face (Fig.6). The PIV measurements were carried out for three different longitudinal positions of the helicopter (X/R = -1, 0, 1) at $Z/R = 2$ and $Y/R = 0$, as given in test 2. Figure 10 presents the velocity field time-averaged over 100 image pairs. The measured flow fields are visualised by means of the in-plane velocity magnitude contours and in-plane streamlines patterns.

Figure 10a clearly shows a high-speed layer issued from the roof edge, with the model positioned at $X/R = -1$. This layer originated from the boundary layer produced by the rotor wake and induced a large recirculating region (clockwise in the figure) ahead of the front face.

For the test condition at $X/R = 0$, just half of the rotor wake impinged the building model roof, as shown by the corresponding pressure pattern of Fig. 9. A clockwise recirculation region produced by the flow blowing from the roof was observed also in this case (Fig. 10b). This recirculation cell was affected by the aft portion of the rotor wake, which was highlighted by the high-velocity slipstream in the top-right corner of the measurement window.

A completely different behaviour was observed under the last condition ($X/R = 1$), where the flow topology in the measurement area showed a counterclockwise recirculation region bounded by a high-velocity region corresponding to the rotor fore streamtube boundary (Fig. 10c). The behaviour of the measured flow field was similar to the wake of an isolated rotor under ground effect, as observed by Fradenburgh [19] and Nathan and Green [20].

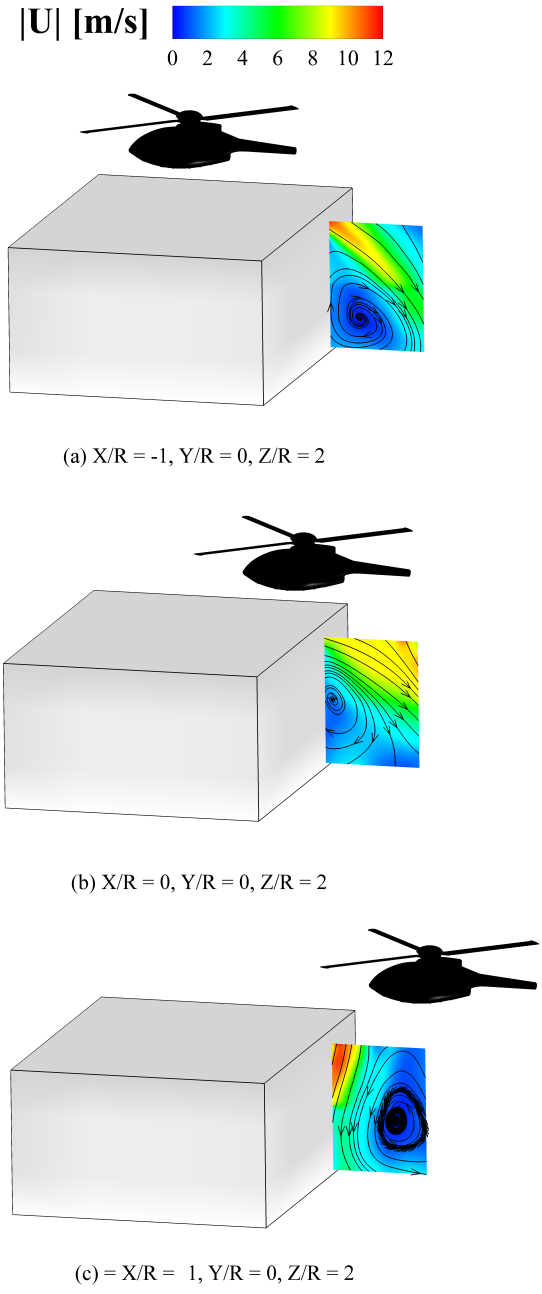

Figure 10: PIV results for test 2 conditions: velocity magnitude contours and in-plane streamlines.

5 CONCLUSIONS

In the present study, a new experimental setup for investigating the aerodynamic interaction between a helicopter and ground obstacles in both windy and not windy condition was presented. The experimental setup basically comprised a motorized helicopter model with a six-component balance and a building model with pressure taps. PIV surveys were carried out in different configurations to clarify the involved flow physics. Some test without wind were carried out as a preliminary assessment of the experimental set-up.

First a ground effect test without the building model was conducted in order to produce a set of reference conditions. The results showed very good agreement in terms of C_t with data from past literature for a similar test configuration, which assessed the experimental setup.

A set of tests was then carried out in order to investigate the helicopter–building interference effects. A test representing an horizontal approach showed a gradual decrease in C_t as the helicopter moved away from the building, because the percentage of the roof inside the slipstream progressively decreased.

This last test was also subject to a PIV survey. A recirculating region, whose topology and morphology were highly dependent on the helicopter position, was found on the side of the building. In particular, the observed flow structure originated from the rotor wake deflection on the upper surface of the building model. For the most external condition that was tested, the typical flow morphology of the ground effect could be observed.

In summary, after the assessment of the test rig and of the measurement chain, the current setup is now ready for tests in more realistic conditions, i.e. in presence of wind. Further developments may be the investigation of the interaction with more defined obstacles such as ships, platforms, etc.

Copyright Statement

References

[1] International Helicopter Safety Team. The U.S. JHSAT Baseline of Helicopter Accident Analysis, `www.ihst.org/portals/54/US_JSHAT_Compendium_Report1.pdf`, 2011.

[2] Federal Aviation Administration. Helicopter Flying Handbook, FAA-H-8083-21A, USA, 2012

[3] Crozon C, Steijl R and Barakos G.N. Numerical Studies of Rotors in Ship Airwake, *39th European Rotorcraft Forum*, Moscow, 3-6 September 2013.

[4] Alpman E, Long LN, Bridges DO and Horn JH. Fully-Coupled Simulations of the Rotorcraft / Ship Dynamic Interface, *AHS International 63rd Annual Forum & Technology Display*, Virginia Beach, VA, USA, 1-3 May 2007.

[5] Timm GK. Obstacle-Induced Flow Recirculation, *Journal of the American Helicopter Society* 1965; 10:1-5.

[6] Lee RG and Zan SJ. Wind Tunnel Testing of a Helicopter Fuselage and Rotor in a Ship Airwake, *29th European Rotorcraft Forum*, Friedrichshafen, Germany, 16-18 September 2003.

[7] Lee RG and Zan SJ. Wind Tunnel Testing to Determine Unsteady Loads on a Helicopter Fuselage in a Ship Airwake, *23rd International Congress of Aeronautical Sciences*, Toronto, Canada, 8-13 September 2002.

[8] Zan SJ. Experimental determination of rotor thrust in a ship airwake. *Journal of the American Helicopter Society*, 47(2), 100-108, 2002.

[9] Nacakli Y and Landman D. Helicopter Downwash/Frigate Airwake Interaction Flowfield PIV Surveys in a Low Speed Wind Tunnel, *AHS International 67th Annual Forum & Technology Display*, Virginia Beach, VA, USA, 3-5 May 2011.

[10] Rajagopalan G, Niazi S, Wadcock AJ, Yamauchi GK and Silva MJ. Experimental and computational Study of the Interaction Between a Tandem-Rotor Helicopter and a Ship, *American Helicopter Society 61st Annual Forum*, Gravepine, TX, USA, 1-3 June 2005.

[11] Quinliven TA and Long KR. Rotor Performance in the Wake of a Large Structure, *American Helicopter Society 61st Annual Forum*, Gravepine, TX, USA, 1-3 June 2005.

[12] Polsky SA and Wilkinson CH, A Computational Study of Outwash for a Helicopter Operating Near a Vertical Face with Comparison to Experimental Data, *AIAA Modeling and Simulation Technologies Conference*, Chicago, IL, USA, 10-13 August 2009.

[13] Pahlke K. GARTEUR Helicopter Cooperative Research, *36th European Rotorcraft Forum*, Paris, France, 7-9 September 2010.

[14] Polak DR, Werner R and Albert RG. Effects of an image plane on the tiltrotor fountain flow. *Journal of the American Helicopter Society*, 45(2), 90-96, 2000.

[15] Polak DR and George AR. (1998). Flowfield and acoustic measurements from a model tiltrotor in hover, *Journal of aircraft*, 35(6), 921-929, 1998.

[16] PIVview 2C version 3.0, User Manual, PIVTEC, www.pivtec.com.

[17] Gibertini G, Gasparini L, and Zasso, A. Aerodynamic design of a civil-aeronautical low speed large wind tunnel. In AGARD conference proceedings (pp. 6-1), AGARD, 1997 .

[18] Leishman J. Principles of helicopter aerodynamics. *Cambridge University Press* 2006.

[19] Fradenburgh EA. The helicopter and the ground effect machine. *Journal of the American Helicopter Society*, 5(4): 24-33, 1960.

[20] Nathan ND and Green RB. The flow around a model helicopter main rotor in ground effect. *Experiments in fluids*, 52(1): 151-166. 2012.